Soft Matter

Accepted Manuscript

ROYAL SOCIETY OF CHEMISTRY

www.rsc.org/softmatter

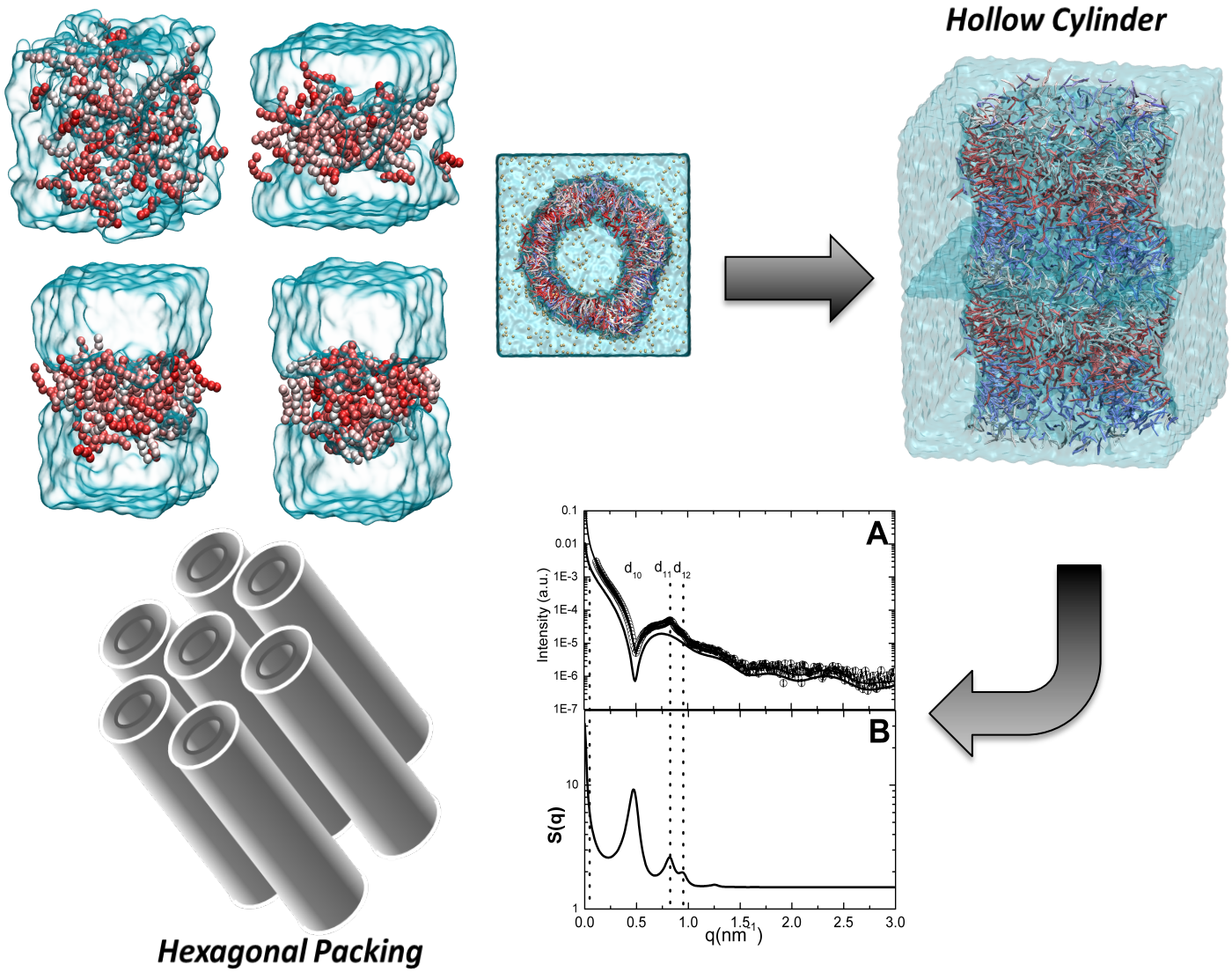

Highlight:

Grown Hormone release Peptide-6 self-assemble into long hollow-cylinders, as evidenced by electron microscopy, Small-angle X-ray Scattering and molecular dynamics simulations.

How does Growth Hormone Releasing Hexapeptide self-assemble in Nanotubes?

Héctor Santana[1], Cesar L. Avila[2], Ingrid Cabrera[3,4], Rolando Páez[1], Viviana Falcón[1], Adalberto Pessoa Jr.[5], Nora Ventosa[3,4], Jaume Veciana[3,4], Rosangela Itri[6], Leandro Ramos Souza Barbosa[6,*]

1 – Department of Pharmaceutical Technology, Center for Genetic Engineering and Biotechnology, Ave 31/158 and 190, PO Box. 6162, Havana 10600, Cuba.

2 – Instituto Superior de Investigaciones Biológicas (INSIBIO), CCT-Tucumán and Instituto de Química Biológica Dr Bernabé Bloj (CONICET-UNT) Chacabuco 461 (T4000ILI) Tucumán, Argentina.

3- Department of Molecular Nanoscience and Organic Materials (ICMAB-CSIC), Bellaterra, 08193, Spain.

4 – CIBER de Bioingeniería, Biomateriales y Nanomedicina (CIBER-BBN), Bellaterra, 08193, Spain.

5 – Department of Biochemical and Pharmaceutical Sciences, School of Pharmaceutical Sciences, University of São Paulo, Brazil.

6 – Instituto de Física, Universidade de São Paulo, *Cx. Postal 66318, CEP 05315-970,* São Paulo, Brazil.

[†]These authors contributed equally to this paper.

* Corresponding author. E-mail: lbarbosa@if.usp.br. Phone: + 55 11 30917157.

Keywords: GHRP-6, SAXS, TEM, MD Simulations, peptide self-assembling; Nanotechnology

Abstract

Growth hormone releasing peptide, GHRP-6, a hexapeptide (His-(D-Trp)-Ala-Trp-(D-Phe)-Lys-NH_2, MW = 872.44 Da) that belongs to a class of synthetic growth hormone secretagogues, can stimulate growth hormone secretion from somatotrophs in several species including humans. In the present study, we demonstrate that GHRP-6 dispersed in aqueous solution, at pH 7.0, room temperature of 22 ^{o}C, is able to form long nanotubes by combining small angle X-ray scattering (SAXS), transmission electron microscopy and molecular dynamic simulation results. Such nanotubes possess inner and outer cross-sections equal to 6.7(2) nm and 13.4(5) nm, respectively. The mechanism of peptide self-assembling was determined by molecular dynamic simulations revealing that the peptides self-assemble like amphiphilic molecules in aqueous solution in a partially interdigitated structure. In this case, the position of the positively charged amino termini is located at the peptide water interface, whereas the neutral NH_2-capped carboxi termini remains buried at the hydrophobic core. On the contrary, the long side chain of Lys-6 stretches out of the hydrophobic core positioning their positive charge near the cylinder surface. The peptide configuration in the nanotube wall comes from the interplay between the hydrophobic interactions of the aromatic side chains of the GHRP-6 and the electrostatic repulsion of its cationic charges. Increasing the peptide concentration, the long nanotubes self-arrange in solution displaying a bi-dimensional hexagonal-like packing in the SAXS curves, with a center-to-center distance of ~ 15 nm. Further, we also show that the nanostructure formed in solution is quite stable being preserved following transfer to solid support.

1. Introduction

Molecular self-assembling is one of the most powerful approaches nowadays to construct advanced functional biomaterials of nanoscale dimension[1,2,3]. Among several different molecules, peptides are outlined as excellent building-blocks for nanotechnology applications, due to their well-known synthesis, small size, chemical flexibility and versatility, biocompatibility, biological recognition abilities and relatively easy chemical and biological modifiability[4,5]. For instance, the structural properties of self-assembled peptides have been exploited due to the formation of quite different structures as nanotubes[6,7], nanospheres, nanofibers[8] , scaffolds[9,10], nanoribbons[11], nanotapes[12], hydrogels[13,14], or even self-assembled vesicle-capped nanotubes that can be selectively disassembled by irradiation as reported by Coleman et al.[15].

Besides their nanotechnological relevance, self-assembled peptides have also been implicated in the health sciences for therapeutic and diagnosis applications[16], as well as for cosmetic application[17]. Some peptides have also the ability to form fibers and gels, composed of elongated structures (like micelles), which could be used for tissue engineering and regenerative medicine applications[16,18].

On this scenario, Growth Hormone Releasing Hexapeptide, GHRP-6 (Fig. 1), belongs to a class of synthetic growth hormone secretagogues (GHSs), which stimulate growth hormone (GH) releasing from somatotrophs in a dose-dependent manner in several species including humans[19]. There are some indications of a potential therapeutic option of GHRP-6 in the prevention and treatment of heart failure[20,21], an effect that seems to be related to an enhanced non-ischemic compensatory mechanism and mediated via specific GH secretagogue receptors rather than via the GH/IGF-1 pathway. Besides, a recent study indicates that the combined administration of GHRP-6 peptide and EGF (epidermal growth factor), which can prevent cell from apoptosis[22], resulted in an effective alternative for the recovery of the amyotrophic lateral sclerosis (ALS)[23], although further preclinical investigations must be carried on[23]. Of note, ALS is a central nervous system (CNS) disease characterized by irreversible loss of spinal motor neurons with an evolution of the patient to death in few years[24,25], with no effective treatment reported up to now.

In spite of the relevance of GHRP-6, there is a lack in the literature concerning its probable self-organization in the physiological environment. In this context, in the current study we focus our attention on the properties of GHRP-6 self-assembling in aqueous solution combining experimental and molecular dynamic (MD) simulation data. The self-aggregation features of GHRP-6 dispersed in phosphate buffer solution, at pH 7.4, were investigated by small angle X-ray scattering (SAXS) technique combined with cryogenic and conventional Transmission Electron Microscopy (Cryo-TEM and TEM) performed on dried samples. SAXS is a low-resolution technique that allows us accessing both the shape and dimension of the scattering object, whereas Cryo-TEM and TEM can reveal small morphological changes as, for instance, twisted-to-helical transition as reported elsewhere[26]. The results revealed that GHRP-6 peptides form elongated linear structures with inner and outer cross-sections of 7 (1) and 13 (1) nm, respectively. Such dimensions were used as constraints to infer the self-assembling mechanism at molecular level by MD. Interestingly, MD evidenced a partially interdigitated peptide in a nanotube-like configuration, resulting from the interplay between the hydrophobic interactions of the aromatic side chains of the GHRP-6 and the electrostatic repulsion of the cationic charges (Fig. 1). The knowledge of the peptide self-assembling mechanism can pave the way for future bio-inspired materials with potential technological applications.

2. Materials and Methods

2.1. Sample Preparation

GHRP-6 was obtained from BCN PEPTIDES (Barcelona, Spain) as the acetate salt and used as received. The GHRP-6 solutions were prepared by dissolving the desired amount of peptide in 20 mM phosphate buffer at pH 7.4. GHRP-6 concentration was determined from UV-Vis spectrometric measurements at 280 nm, using the molar extinction coefficient obtained from the amino acid composition (ε_{280} = 11,120 $M^{-1}cm^{-1}$). For TEM and Cryo-TEM analysis the samples were incubated at room temperature of 22 ºC for about one day prior to the measurements. All reagents were of analytical grade and used without further purification.

2.2. Transmission Electron Microscopy

TEM negative staining was performed as follows: a former layer on a copper grid was coated with carbon. The grid was immersed in 20 µl of the sample and blotted after 1 min. The grid was washed with water for 1 min and then blotted to remove excess of protein material. To enhance the contrast, the grid was immersed in 2% (w/w) uranyl acetate and blotted after 1 min. Examination was performed using a JEOL JEM-2000 EX transmission electron microscope (JEOL LTD., Tokio, Japan) operating at 80 kV.

Cryo-TEM images were obtained using a JEOL JEM-2011 transmission electron microscope (JEOL LTD., Tokio, Japan) operating at 120 kV. A small drop of sample was placed on a copper grid coated with a perforated polymer film. Excess solution was thereafter removed by blotting with filter paper. Immediately after film preparation, the grid was plunged into liquid ethane held at a temperature just above its freezing point (94 K). The vitrified sample was then transferred to the microscope for analysis. To prevent sample perturbation and the formation of ice crystals, the specimens were kept cold (77 K) during both the transfer and viewing procedures. Samples composed of 20 mg/mL of GHRP-6 peptides in phosphate buffer solution, pH 7.4, were submitted to TEM and Cryo-TEM measurements after incubation for about one day at temperatures from 2 to 8 ºC.

TEM and Cryo-TEM images were analyzed Using Gatan Digital Micrograph 1.8 software. The tools of this software allowed us to measure both inner and outer cross-sections of each aggregate independently. Accordingly, histograms and corresponding Gaussian fits were obtained by using OriginPro 8.0. A total of 85 and 40 linear aggregates were analyzed through Cryo-TEM and TEM images, respectively.

2.3. Small-angle X-ray Scattering

Small Angle X-ray Scattering (SAXS) data from phosphate buffer solutions containing GHRP-6 at 20, 30, 50 and 70 mg/mL, pH 7.4, were obtained on the SAXS2 beamline at the *Laboratório Nacional de Luz Síncrotron* (LNLS, Campinas, Brazil). The radiation wavelength was set to 0.148 nm and a MarCCD detector (bi-dimensional position-sensitive detector) was used to record the scattering patterns. The sample-to-detector distance was set to ~ 1000 mm allowing us to explore a scattering vector interval from 0.11 to 3.3 nm^{-1}, where q is the magnitude of the scattering q-vector defined by $q = (4\pi/\lambda)\sin\theta$ (being 2θ the scattering angle). In this way, the maximum Bragg distance accessible from our experimental set-up was *circa* 60 nm.

Samples were set between two mica windows and a 1 mm spacer, handled in a liquid sample-holder placed perpendicular to the incoming beam. The obtained curves (data collection of 5 minutes) were normalized by taking into account the X-ray beam intensity decrease during the experiment. The scattering curve of the phosphate buffer solution was subtracted from the samples SAXS curves, considering each sample's attenuation. All measurements were taken at room temperature of 22 ^{o}C.

For the SAXS data analysis we here assume that the scattering objects can be represented by hollow cylinders as nanotubes. It is worthy of note that such a cylindrical symmetry for the peptide aggregates is further confirmed by molecular dynamic simulations. Therefore, the SAXS intensity *I(q)* from a solution of long cylinders such that $L >> 10D_{cs}$, where L and D_{cs} are the cylinder length and cross-section diameter, respectively, can be written as [27,28]:

$$I(q) = k\, n_p\, P(q)\, S(q), \quad (1)$$

where n_p corresponds to the particle number density and k is a normalization factor related to the instrumental effects. The *P(q)* and *S(q)* in Eq. (1) are the scattering particle form factor and structure factor, respectively. In our case, the *P(q)* function parameters for long hollow cylinders are the inner and outer cylinder radii, namely, R_{in} and R_{out}, respectively, which define the layer thickness ($=R_{out} - R_{in}$) comprising the peptides and hydration water[27,28]. Furthermore, this model is implemented in GENFIT software[29]. For a two-dimensional hexagonal lattice with cell parameter *a*, *S(q)* function is correlated to the diffraction Bragg's peaks positions centered at[30].

$$q_{hk} = (4\pi/a\ (3)^{1/2})(h^2+hk+k^2)^{1/2} \quad (2)$$

with *h* and *k,* the Miller indices. Therefore, in this case, the scattering intensity exhibits Bragg peaks, which positions in the reciprocal space relative to the position of the first peak are 1, $\sqrt{3}$, 2, $\sqrt{7}$ and so on, corresponding to d_{10}, d_{11}, d_{20}, d_{21} interplanar distances, respectively ($d_{hk}=2\pi/q_{hk}$).

Interestingly, Freiberger and Glatter[30] described the scattering intensity of hexagonal-like arrangement exhibiting pronounced Bragg peaks dependent on both the height and width of the Bragg peaks. This was named as the multi-peak Model, first derived by Forster et al.[31] and implemented in the GIFT (Generalized Inverse Fourier Transform) software[30]. According to such methodology, it is possible to derive the number of coherent scattering cylinders and the degree of disorder caused, for instance, by thermal fluctuations[30,31]

Here we made use of such methodology in such a way that the fitting parameters to the SAXS experimental data are: the cylinder cross-section dimension, the cylinder-cylinder mean distance corresponding to the lattice constant *a*, and the lattice vibrations related to the thermal vibrations. Noteworthy, thermal vibrations can be understood as distortions on the lattice position of the rigid cylinders. Such distortions are understood as oscillations around an equilibrium position, giving rise to a relative mean square displacement, σ_a^r. Thus, the final fitting parameter is the total mean square displacement, σ_a, which can be written as $\sigma_a = a\sigma_a^r$ [31]. Finally, as in the proposed model the cylinder is much longer than its cross-section dimension, the latter is considered to be monodisperse[30]. A more detailed description of this model can be found elsewhere[30, 31].

2.4 Molecular dynamic simulation

The self-organizing properties of the GHRP-6 peptide were evaluated using coarse-grained molecular dynamic (CG-MD) simulations using the MARTINI forcefield[32] and its extension to proteins[33], as implemented in the Gromacs 4 package[34]. The systems were simulated using a 20 fs timestep, under NPT conditions using Berendsen thermostat and barostat.

Simulations were conducted starting from random distribution of the peptides on a cubic water box with phosphate ions to neutralize the system and to mimic the experimental conditions. Thus, following such procedure, it is possible to get more details on the peptide behavior during the self-assembling process. Additional simulations were started from the peptide aggregates reorganized into pentagonal arrangements.

3. Results

3.1 Cryo - and conventional Transmission Electron Microscopy

Cryo-TEM (Figures 2A, 2B and 2C) and TEM (Figure 2D) micrographs obtained from samples composed of 20 mg/mL of GHRP-6, in the presence of phosphate buffer at pH 7.4, reveal that bundles of long linear structures are formed. Furthermore, a magnification of part of such structures is displayed on Fig. 2B, evidencing a lower electron density region along the longitudinal direction in respect to the outer region of the peptide aggregate. Such finding can be associated with the formation of hollow aggregates. This point will be better explored by means of SAXS measurements and molecular dynamic simulations later on the text.

Figures 2E and 2F depict the inner and the outer cross-section dimensions of the linear aggregates with the best Gaussian fits (solid lines) to the histograms for the cryo-TEM and TEM analysis, respectively. Such values as well as the corresponding thicknesses of the aggregates are displayed in Table 1. As one can observe from the Figs. 2E and 2F, the distribution of the cross-section dimensions of the GHRP-6 aggregates is quite monodisperse. According to TEM, the outer and inner dimensions are 14.2(6) and 7.0(7) nm, respectively (Fig. 2E), whereas the thickness amounts to 3.6(3) nm. Regarding Cryo-TEM measurements, the outer and inner cross-section dimensions and the thickness are 11.9(8), 5.8(7) and 3.1(4) nm (Fig. 2F), respectively.

With the aim of better evaluating the main structural features of the peptide aggregate as well as the mechanism that promotes its self-assembling, small-angle X-ray scattering experiments and molecular dynamic simulation were thus carried out, as follows.

3.2 SAXS

SAXS measurements were performed at peptide concentration ranging from 20 to 70 mg/ml at pH 7.4 in 20 mM phosphate buffer. Samples with smaller concentrations did not result in a detectable SAXS signal after one day of sample preparation. Figure 3A shows the scattering curve from 20 mg/mL of GHRP-6 along with the best model fitting supposing that the peptides self-assemble into long hollow cylinder-like aggregates, which represent the hollow linear structures observed by electron microscopy (Fig. 2). Of note, a homogeneous cylinder model was also employed as an attempt to fit the experimental data. Nevertheless, it failed to reproduce the

broad peak centered at q ~ 0.75 nm^{-1} in the scattering curve (data not shown). Such a broad peak is typical from the scattering of either hollow or core-shell structures [35,36].

According to the modeling, the cylinder inner radius and the peptide-containing shell thickness resulted to be, respectively, 3.7(2) nm and 3.0(2) nm (inset on Figure 3A), which indicated an outer cylinder cross-section of 6.7(2) nm, in good agreement with electron microscopy results (Table 1). In this way, the cylinder wall thickness of 3.0(2) nm determined by SAXS could accommodate two GHRP-6 molecules partially stacked or interpenetrated, considering that the extended length of GHRP-6 molecule is ~ 2 nm, calculated from the C_α of His1 to the C_α of Lis6 as measured with VMD software, see scheme 1). Thus, it is possible that GHRP-6 behaves as a surfactant-like peptide, i.e., it self-assembles in bilayers on the cylinder wall, resulting in a nanotube-like aggregate of total external diameter of ~ 13.4(5) nm. We will return to this point when discussing molecular dynamic simulations results later on in the paper.

As the GHRP-6 concentration increases from 30 mg/mL to 70 mg/mL (Fig. 3B) it is possible to notice the appearance of Bragg peaks at q ~ 0.83 nm^{-1} and 0.96 nm^{-1} in the normalized SAXS curves (arrows in Fig 3B). Interestingly, the SAXS curves profiles are not affected by increasing the peptide amount. One should bear in mind that the peak position defines the average distance among the interacting structures, which in the present study is the hollow-cylinder center-to-center position. Thus, as the Bragg peaks position remains unaltered when the peptide concentration increases, the mean distance between the center-to-center hollow-cylinders also remains the same regardless the GHRP-6 concentration. Therefore, an increase in the peptide concentration conducts to an increase in the nanotube long dimension, without affecting its cross-section.

Regarding the position of the Bragg peaks, if we consider the first diffraction peak centered at q ~ 0.83 nm^{-1}, the mean distance between the interacting nanotubes would be smaller than their cross-section with no physical meaning. On the other hand, with the assumption of these two peaks (arrows on Fig. 3B) correspond, indeed, to a second and third order of a local hexagonal liquid-crystal packing, the first diffraction peak should lie at q_{10} = 0.48 nm^{-1}, which is very close to the minimum of the hollow-cylinder form factor at q ~ 0.5 nm^{-1} (Fig. 4A). Thereby, the experimental diffraction peaks observed at q ~ 0.83 nm^{-1} and 0.96 nm^{-1} are related to the (11) and (20) plane reflections of the hexagonal 2D-packing (Fig. 4A). The dashed-vertical lines on Fig 3A evidence the position of the first three peaks from a hexagonal arrangement. In order to

better infer some physical parameters to the hexagonal packing, we use the methodology developed by Freiberger and Glatter[30] to analyse the SAXS curves by retrieving the S(q) and P(q) functions, concomitantly.

By doing so, Figure 4A shows the best fitting (solid line) to the SAXS data from 70 mg/mL GHRP-6 dispersed in aqueous solution along with the P(q) function (dashed line), as an example, whereas Fig. 4B displays the resulting S(q) function, with the following parameters: the lattice parameter, a = 15.2 nm, the domain size D ~ 63 nm, and the mean lattice deviation σ_a ~ 1.8 nm, whereas the cylinder cross-section was 13.4(5)nm, in accordance to SAXS result. As one can note, the main peak of the S(q) function is indeed coincident with the minimum of the P(q) function. The corresponding unit cell parameter a of 15.2 nm related to the center-to-center distance between two adjacent hollow-cylinders (see scheme in the inset of Fig 4A) indicates a water layer of *circa* 1.4(5) nm separating two adjacent nanotubes (i.e. the wall-to-wall distance), taking into account that the total cylinder cross-section dimension is around ~ 13.4(5) nm. Such a finding reveals a quite narrow water interface between the hollow cylinders. Besides, the domain size (~ 63 nm) is on the same order of magnitude that the lattice parameter a (~ 15.2 nm), suggesting that there are a small number of interacting cylinders, which is also justified by the broad Bragg peaks (see scheme in the inset of Fig. 4B). In fact, using a rough approximation, from the domain size, D, combined with the unit cell dimension, a, it is possible to suggest that an average number of ~ 13 cylinders in solution are short-ranged correlated giving rise to the hexagonal-like pattern observed. Noteworthy, the structural features of the peptides remain unaltered, despite the changes in the peptide concentration.

Furthermore, the intensities of the high-order reflections are damped due to deviations from the ideal lattice positions[31]. Such deviations can be mathematically modeled using the Debye-Weller factor, as described elsewhere[31]. In the present study, such deviations are mainly due to thermal fluctuations of the cylinders mean positions being equal to ~1.8 nm, in accordance with the mean wall-to-wall distance among the adjacent cylinders. Taking together, the SAXS results indicate that the hollow-cylinders are interacting with an average distance slightly larger than the hollow-cylinder cross-section comprising a quite small bundle of cylinders.

The agreement between SAXS and the transmission electron microscopies results is quite remarkable, as shown in Table 1. From TEM values obtained over dried samples and Cryo-TEM

data collect over quickly-frozen samples without the solvent removal, we can infer that the GHRP-6 aggregates keep their structure following transfer from aqueous solution to solid support.

3.3 Molecular dynamics simulation

Modeling self-assembly of molecules at the atomic level using computational techniques has remained a challenge, due to the time scales needed to simulate the process, in the order of micro to mili seconds, and the large number of particles involved. In this regard, the development of coarse grained force fields using either implicit or explicit water for the representation of the system made it possible to model the self-assembly of lipid [37], peptides[38, 39], and proteins[40]. Among all the coarse-grained models developed for proteins, nicely reviewed by Tozini[40] we chose the MARTINI force-field[32,33] which has been proven to be useful in reproducing the assemble properties of several biomolecular systems[33]. This coarse-grained force field offers the possibility to perform unconstrained MD simulations of the assembly process providing an unbiased sampling. Briefly, the force field maps four heavy atoms into one interaction particle and has been parametrized focusing on reproducing the partition free energy between apolar and polar phases. The simplifications introduced in the representation of the system, provides a four-fold speed-up factor when compared with all-atom simulations. In this work we use this effective time that has been estimated based on the diffusion coefficient of coarse-grained water compared to real water.

Figure 5A-D depicts the time evolution of a peptide solution starting from random positions (Fig 5A), showing that as soon as 2 μs (Fig. 5D) a phase separation between GHRP-6 and water takes place. Furthermore, its cross section has a circular shape, resembling the structure assumed in SAXS data analysis. Nevertheless, it is not possible, with such information, to describe the peptide-peptide interaction that lead to such arrangement. This point will be better discussed latter on in the text.

To further evaluate the structural properties of the peptide within a cylindrical arrangement, the peptide layer was replicated using a cylindrical symmetry along the z-axis and simulated for additional 100 μs (Fig 5E and 5F). This procedure was made to guarantee that such arrangement is stable at longer times, i.e. 100 μs. Interesting, after a period of ~ 20 μs the

structure is stable, and within the remaining 80 μs no significant changes were found. In contrast to the smaller system described above, an ordering of the peptide within the hollow-cylinder becomes evident, as shown in Fig. 5F.

The radial distribution function, g(r), is a powerful tool to study the mean distance between different residues or even atoms, in order to get further information on the peptide organization within the cylinder wall. On this ground, Figure 6A shows the g(r) function from the cylinder's center of mass for some relevant components of the system. The inner and outer radii of the hollow cylinder, taken from the peaks in the distribution of the outermost layer of the peptide, are 4.5 nm and 7.5 nm respectively. It is quite impressive the similitude in the cylinder's wall thickness (3.0 nm), among all experimental and theoretical approaches, see Table 1. It thus suggests that even though there might be a slight deviation in the packing of the peptides, this simplified theoretical model is able to reproduce the probable distribution of the peptide within the nanotube wall. The external and internal walls of the cylinder, corresponding to the peptide/water interface, are preferentially populated with the amino termini of the peptide, while the amide-capped carboxy termini remains buried within the core of the cylinder. Although the core is hydrophobic, as denoted by the absence of water between 5 and 7 nm in g(r) (Fig. 6A), the positive charges of the amino group in the side chain of Lys stretch out to the peptide/water interface where it is neutralized by phosphate ions. The arrangement of the Lys side chain is reminiscent of the snorkeling behavior described in transmembrane helices embedded in lipidic membranes[41]. An ordering of the peptides into the nanotube wall is also noticed when analyzing the orientation of the vector defined along the peptide chain as compared with that at radial direction, from the cylinder's center of mass up to the peptide's center of mass (Fig. 6B). Figure 6B shows the probability distribution function of the angle formed between these two vectors for all peptides during the last 20 μs of simulation. There are two peaks in the distribution, 0 and π radians, corresponding to the peptides pointing inside/outside the cylinder's center of mass, respectively. Such an analysis indicates that the peptide is pointing parallel to the radial direction (Fig. 6B).

Fig 6C shows the electron density map along the cylinder's cross-section, showing the N-termini (blue channel) at the water/peptide interface, while the C-termini (green channel) is located in the core. Thus, taking together, these results indicate that GHRP-6 behaves like an amphiphilic molecule in solution, forming a partially interdigitated wall, where the N-termini

located at the peptide/water interface (His residue) and the C-termini at the core (Lys residue); while the positive charges arising from NH_3 from the inner Lys groups are neutralized by phosphate ions. Furthermore, Fig. 6D shows the probability density function, P(**r**) calculated for the peptides within the hollow-cylinder wall. The average value is 1.53(6) nm, and one can notice an asymmetrical distribution for P(**r**) (Fig. 6D).

Noteworthy, the hexagonal arrangement for the cylinders at higher concentrations, evidenced by SAXS, could be explained based on the charge distribution within the cylinder wall, i.e., the positive His residues are neutralized by the phosphate ions at the surface, favoring the cylinder-cylinder interaction, giving rise to the hexagonal arrangement evidenced by SAXS.

4. Discussion

There is a large amount of research dealing with the self-assembling properties of peptides in solution due to the emergent biotechnological applications[1, 17, 42, 43]. Interestingly, in a pioneer work, Santoso et al.[44] studied the self-assembling properties of surfactant-like peptides with different Glycine (from 4 up to 10 residues) tails (corresponding to the hydrophobic portion) and aspartic acid as the constituent of the negatively charged polar headgroup[44]. The authors evidenced that all studied molecules formed either nanotubes or nanovesicles in solution. Moreover, the polydispersity of these structures was dependent on the length of the Glycine tail[44], and in general their cross section is found to be ~ 50 nm. In our case, GHRP-6 forms thinner hollow-cylinders which are monodisperse in size.

Cenker et al.[45] , on the other hand, studied the influence of trifluoroacetate (TFA) salt on the heptapeptide $(ala)_6lys$, which has six alanine residues forming the peptide "hydrophobic tail" and one lysine residue representing the polar head group. The authors evidenced that the peptides self-assemble as hollow cylinders with an inner radius of *circa* 26.0(1.3) nm and a wall thickness < 1.0 nm[45]. The self-assembly is highly cooperative and the peptides are distributed in a two-dimensional crystal, which is cylindrically bent[45], with the peptide aligned along the cylinder surface and perpendicularly to the radial direction. Thus, the observed small wall thickness is due to the relative position of the peptide in the hollow cylinder wall. One should bear in mind that although $(ala)_6lys$ is an amphiphilic molecule, it has not a surfactant-like behavior in the cylinder wall. For instance, Middleton at al.[7] obtained similar results, when studied the architecture of

peptides nanotubes formed by the same heptapeptide $(ala)_6lys$ using solid state nuclear magnetic resonance, SSNMR, Fourier transform infrared spectroscopy, FTIR, and transmission electron microscopy, TEM. The authors evidenced that the $(ala)_6lys$ nanotubes had a cross-section of ~ 23 nm, in accordance to the value observed by Cenker et al.[45]. They also proposed that the peptides self-assemble into nanotubes constructed from monolayers, being the inner water region and the cylinder wall thickness equal to 20 and ~ 3 nm, respectively[7]. In this case, the peptide is also aligned in the cylinder surface, i.e., perpendicular to the cylinder radial direction. Moreover, the authors were also able to infer that the peptides are organized in β-strands conformation with a 4.7 Å strand spacing (antiparallel β -sheets)[7], compatible to the small cylinder wall.

In contrast, in the present study we clearly show that the mechanism of short peptides self-assembling is not general but depends on the peptide amino-acid sequence. In our case, we were able to show that GHRP-6 behaves as an amphiphilic molecule such that the hexapeptide self-assembles parallel to the cylinder radial direction in the non-aqueous environment, forming a quite thinner nanotube in respect to others reported on the literature.

5. Conclusions

In this study we combine bioinformatics with experimental data to investigate how the grown hormone releasing hexapeptide, GHRP-6, does associate in aqueous solution. We experimentally show that at 20 mg/ml GHRP-6 self-assembles into very long hollow-cylinders that are at least a few hundreds nm long after 1 day of sample preparation. According to SAXS technique, for larger peptide concentration (> 30 mg/ml), the shape of the long aggregates remains the same, but bundles of nanotubes are disposed in a hexagonal arrangement in solution, with a very well defined center-to-center distance of ~ 15 nm. Of note, neither twisted nor helical aggregates were observed by electron microscopy as often proposed for amyloid-like peptides[26]. Furthermore, according to molecular dynamic simulations a peptide orientation along the cylinder-shell was proposed to be perpendicular to the cylinder surface, similar to an interdigitated bilayer as depicted in Fig 6E. Thus, GHRP-6 can be considered as an amphiphilic hexapeptide with two charged groups at physiological pH (corresponding to the NH3 groups at the N-termini and the Lys sidechain) located in the ends of the polypeptide chain and one hydrophobic core composed by four residues (DTrp-Ala-Trp-DPhe) (Fig 1). Such composition is

probable responsible for the interdigitation, since both charges should be partially exposed to water (Fig 6E).

Acknowledgments:

Authors thank CNPq, and FAPESP for financial support. The authors are also in debt with prof. Paolo Mariani and Francesco Spinozzi, both from Università Politecnica delle Marche, Ancona, Italy, who provided us the GENFIT software. RI and LRSB are recipients from CNPq research fellowship. IC, NV and JV acknowledge financial support from Instituto de Salud Carlos III, through "Acciones CIBER". The Networking Research Center on Bioengineering, Biomaterials and Nanomedicine(CIBER-BBN) is an initiative funded by the VI National R&D&I Plan 2008-2011, Iniciativa Ingenio 2010, Consolider Program, CIBER Actions and financed by the Instituto de Salud Carlos III with assistance from the European Regional Development Fund. Technical support from SAXS beam line of the Laboratório Nacional de Luz Síncrotron, LNLS (Brazil) and the Microscopy Service of UAB (Cryo-TEM images (Spain)) are also acknowledged. Scheme 1 was made with VMD software support. VMD is developed with NIH support by the Theoretical and Computational Biophysics group at the Beckman Institute, University of Illinois at Urbana-Champaign.

Table I. Comparison of external and inner cross-sections of GHRP-6 self-assembled aggregate, as well as its thickness, obtained using Cryo-TEM, TEM, SAXS and MDS (molecular dynamic simulation) techniques with the associated standard deviation.

	Cryo-TEM	TEM	SAXS	MDS
External cross-section (nm)	11.9 (8)	14.2 (6)	13.4 (5)	15.0
Inner cross-section (nm)	5.8 (7)	7.0 (7)	7.4 (2)	9.0
Thickness (nm)	3.1 (4)	3.6 (3)	3.0 (2)	3.0

Legend: The values in parenthesis represent the standard deviation

Figure Legends

Figure 1 – Schematic representation of GHRP-6.

Figure 2 - Cryo-Electron Microscopy (A and B and C) and Transmission Electron Microscopy (D) images of GHRP-6, 20 mg/mL in phosphate buffer solution at pH 7.4. Inner (light Grey) and outer (dark grey) cross-section distribution histogram for the linear aggregates obtained with the analysis of TEM (E) and Cryo-TEM (F), respectively. The solid lines in E and F are the best Gaussian fits for each distribution. The adjustment parameters can be appreciated in Table 1.

Figure 3 – (A) Scattering curve from GHRP-6 at 20 mg/ml in phosphate buffer solution (open circles), pH 7.4, along with the best fitting considering a long hollow cylinder-like model (solid line). A schematic representation of the hollow cylinder cross-section can be appreciated in the inset, within the main dimensions of the cylinder. (B) Concentration-normalized SAXS curves of GHRP-6 at 30 (Δ), 50 (∇) and 70 mg/mL (◊) at pH 7.4 in phosphate buffer. The arrows indicate the position of the visible Bragg peaks. See text for further details.

Figure 4 – (A) SAXS curves of GHRP-6 at 70 mg/ml (open spheres) along with the best fitting obtained using the hexagonal model described by Freiberger and Glatter[30], fitting eq. 1 In the inset one can see the average center-to-center distance of each hollow-cylinder. The dotted line (A) is the hollow cylinder form factor, P(q), whereas the solid line in panel B is the cylinder-cylinder interference function, S(q). In the inset of panel B one can see an schematic representation for the average interacting hollow-cylinders within a domain, obtained using the

approach developed by Freiberger and Glatter[30]. The dashed lines show the correspondence between the peaks of the S(q) in B and the experimental scattering curve.

Figure 5 – Snapshots of the spontaneous aggregation of GHRP-6 peptide in a simulation box at (A) 0 ns, (B) 150ns, (C) 300ns and (D) 500ns. (E) Backbone representation of the peptide in a cylindrical aggregate after 20 μs of simulation. (F) Cross-section of the cylinder after 20 μs of simulation. The bar on 5E has 10 nm.

Figure 6 – (A) Radial distribution function g(r) from cylinder's center of mass of selected peptide segments, see figure legend for further details. (B) Probability density distribution of the angle formed between the peptide's longest axis and the radial vector (C) Density map across the plane perpendicular to the cylinder's long axis depicting the mean position of His1 (blue), Lys6 (green) and PHO (red). (D) Probability density function calculated for the GHRP-6 backbone end-to-end distance P(**r**). The mean distance is 1.53(6) nm averaged over time for the all the peptides within the nanotube. (E) Schematic representation of the arrangement of the peptides into the cylinder wall. Phosphate ions are depicted in red, N-termini is depicted in cyan, while Lys side-chain is shown in stick representation.

Legend for the figure 6D: Probability density function calculated for the GHRP-6 backbone end-to-end distance P(r). The mean distance is 1.53 +/- 0.06 nm averaged over time for the all the peptides within the nanotube.

References

1. A. Dehsorkhi, V. Castelletto, I. W. Hamley, J. Seitsonen and J. Ruokolainen, *Langmuir : the ACS journal of surfaces and colloids*, 2013, **29**, 14246-14253.
2. S. Zhang, *Nature biotechnology*, 2003, **21**, 1171-1178.
3. T. A. Doll, S. Raman, R. Dey and P. Burkhard, *Journal of the Royal Society, Interface / the Royal Society*, 2013, **10**, 20120740.
4. M. R. Ghadiri, J. R. Granja, R. A. Milligan, D. E. McRee and N. Khazanovich, *Nature*, 1993, **366**, 324-327.
5. X. Zhao, F. Pan, H. Xu, M. Yaseen, H. Shan, C. A. Hauser, S. Zhang and J. R. Lu, *Chemical Society reviews*, 2010, **39**, 3480-3498.
6. S. Scanlon and A. Aggeli, *Nano Today*, 2008, **3**, 22-30.
7. D. A. Middleton, J. Madine, V. Castelletto and I. W. Hamley, *Angewandte Chemie*, 2013, **52**, 10537-10540.
8. A. Mishra, Y. H. Loo, R. S. Deng, Y. J. Chuah, H. T. Hee, J. Y. Ying and C. A. E. Hauser, *Nano Today*, 2011, **6**, 438-438.
9. Y. L. Yang, U. Khoe, X. M. Wang, A. Horii, H. Yokoi and S. G. Zhang, *Nano Today*, 2009, **4**, 193-210.
10. C. A. E. Hauser and S. G. Zhang, *Chemical Society reviews*, 2010, **39**, 2780-2790.
11. Y. Y. Lin, Y. Qiao, P. F. Tang, Z. B. Li and J. B. Huang, *Soft Matter*, 2011, **7**, 2762-2769.
12. J. F. Miravet, B. Escuder, M. D. Segarra-Maset, M. Tena-Solsona, I. W. Hamley, A. Dehsorkhi and V. Castelletto, *Soft Matter*, 2013, **9**, 3558-3564.
13. A. Mahler, M. Reches, M. Rechter, S. Cohen and E. Gazit, *Adv Mater*, 2006, **18**, 1365-+.
14. G. Fichman and E. Gazit, *Acta biomaterialia*, 2014, **10**, 1671-1682.
15. A. C. Coleman, J. M. Beierle, M. C. Stuart, B. Macia, G. Caroli, J. T. Mika, D. J. van Dijken, J. Chen, W. R. Browne and B. L. Feringa, *Nature nanotechnology*, 2011, **6**, 547-552.
16. A. Trent, R. Marullo, B. Lin, M. Black and M. Tirrell, *Soft Matter*, 2011, **7**, 9572-9582.
17. V. Castelletto, I. W. Hamley, C. Whitehouse, P. J. Matts, R. Osborne and E. S. Baker, *Langmuir : the ACS journal of surfaces and colloids*, 2013, **29**, 9149-9155.
18. I. W. Hamley, *Soft Matter*, 2011, **7**, 4122-4138.
19. K. Cheng, W. W. S. Chan, A. Barreto, E. M. Convey and R. G. Smith, *Endocrinology*, 1989, **124**, 2791-2798.
20. Y. T. Shen, J. J. Lynch, R. J. Hargreaves and R. J. Gould, *J Pharmacol Exp Ther*, 2003, **306**, 815-820.
21. J. Berlanga, D. Cibrian, L. Guevara, H. Dominguez, J. S. Alba, A. Seralena, G. Guillen, E. Lopez-Mola, A. Rodriguez, B. Perez, D. Garcia and N. S. Vispo, *Clin Sci*, 2007, **112**, 241-250.
22. T. Niidome, N. Morimoto, S. Iijima, A. Akaike, T. Kihara and H. Sugimoto, *Eur J Pharmacol*, 2006, **548**, 1-8.
23. D. G. del Barco, H. Perez-Saad, V. Rodriguez, J. Marin, V. Falcon, J. Martin, D. Cibrian and J. Berlanga, *Neurotox Res*, 2011, **19**, 195-209.
24. J. P. Crow, N. Y. Calingasan, J. Y. Chen, J. L. Hill and M. F. Beal, *Ann Neurol*, 2005, **58**, 258-265.

25. E. Beghi, T. Mennini, C. Bendotti, P. Bigini, G. Logroscino, A. Chio, O. Hardiman, D. Mitchell, R. Swingler, B. J. Traynor and A. Al-Chalabi, *Curr Med Chem*, 2007, **14**, 3185-3200.
26. E. T. Pashuck and S. I. Stupp, *J Am Chem Soc*, 2010, **132**, 8819-+.
27. A. Guinier and G. Fournet, *Small-angle scattering of X-rays*, Wiley, New York,, 1955.
28. O. Glatter and O. Kratky, *Small angle x-ray scattering*, Academic Press, London ; New York, 1982.
29. F. Spinozzi, C. Ferrero, M. G. Ortore, A. De Maria Antolinos and P. Mariani, *Journal of applied crystallography*, 2014, **47**, 1132-1139.
30. N. Freiberger and O. Glatter, *The journal of physical chemistry. B*, 2006, **110**, 14719-14727.
31. S. Forster, A. Timmann, M. Konrad, C. Schellbach, A. Meyer, S. S. Funari, P. Mulvaney and R. Knott, *The journal of physical chemistry. B*, 2005, **109**, 1347-1360.
32. S. J. Marrink, H. J. Risselada, S. Yefimov, D. P. Tieleman and A. H. de Vries, *The journal of physical chemistry. B*, 2007, **111**, 7812-7824.
33. L. Monticelli, S. K. Kandasamy, X. Periole, R. G. Larson, D. P. Tieleman and S. J. Marrink, *J Chem Theory Comput*, 2008, **4**, 819-834.
34. B. Hess, C. Kutzner, D. van der Spoel and E. Lindahl, *J Chem Theory Comput*, 2008, **4**, 435-447.
35. C. O. Rangel-Yagui, H. W. Hsu, L. R. Barbosa, W. Caetano, A. Pessoa, Jr., L. C. Tavares and R. Itri, *Pharmaceutical development and technology*, 2007, **12**, 183-192.
36. S. C. Gandini, E. L. Gelamo, R. Itri and M. Tabak, *Biophysical journal*, 2003, **85**, 1259-1268.
37. Y. Wang, J. K. Sigurdsson, E. Brandt and P. J. Atzberger, *Physical Review E*, 2013, **88**, 023301.
38. R. B. Pandey, Z. Kuang and B. L. Farmer, *PLoS ONE*, 2013, **8**, e70847.
39. R. S. Hissam, B. L. Farmer and R. B. Pandey, *Physical Chemistry Chemical Physics*, 2011, **13**, 21262-21272.
40. V. Tozzini, *Current Opinion in Structural Biology*, 2005, **15**, 144-150.
41. E. Strandberg and J. A. Killian, *Febs Lett*, 2003, **544**, 69-73.
42. V. Castelletto, I. W. Hamley, M. D. Segarra-Maset, C. B. Gumbau, J. F. Miravet, B. Escuder, J. Seitsonen and J. Ruokolainen, *Biomacromolecules*, 2014, **15**, 591-598.
43. A. Dehsorkhi, V. Castelletto and I. W. Hamley, *Journal of peptide science : an official publication of the European Peptide Society*, 2014.
44. S. Santoso, W. Hwang, H. Hartman and S. G. Zhang, *Nano Lett*, 2002, **2**, 687-691.
45. C. C. Cenker, S. Bucak and U. Olsson, *Soft Matter*, 2011, **7**, 4868-4875.

TOC

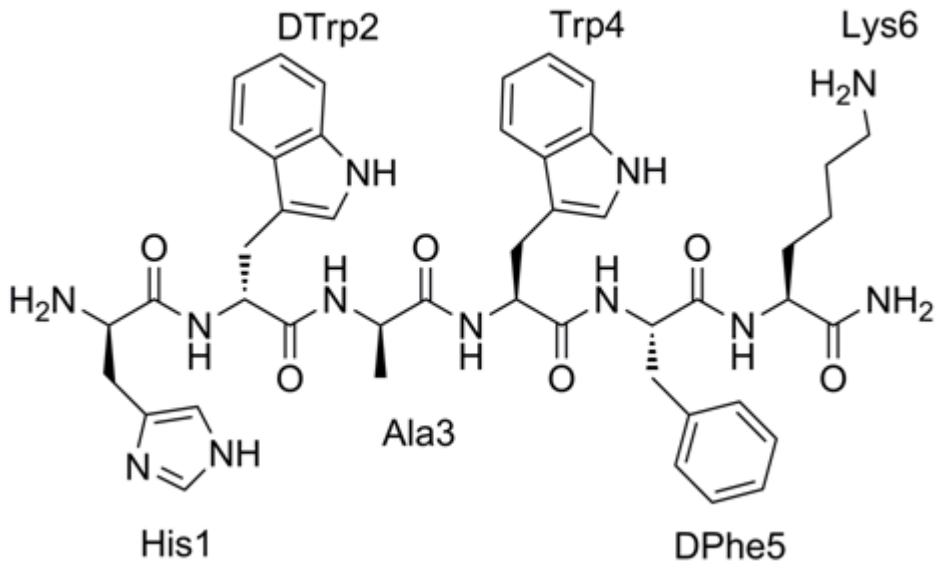

Figure 1

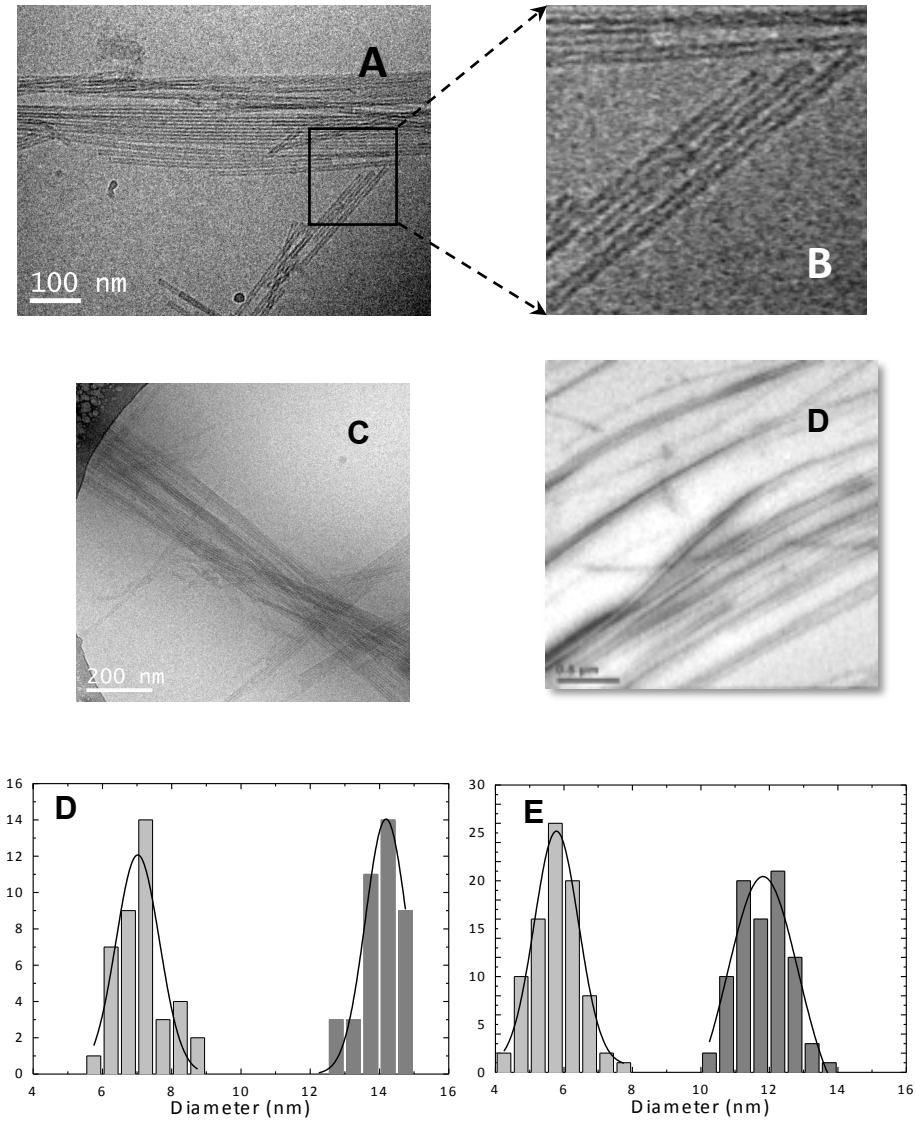

Fig. 2

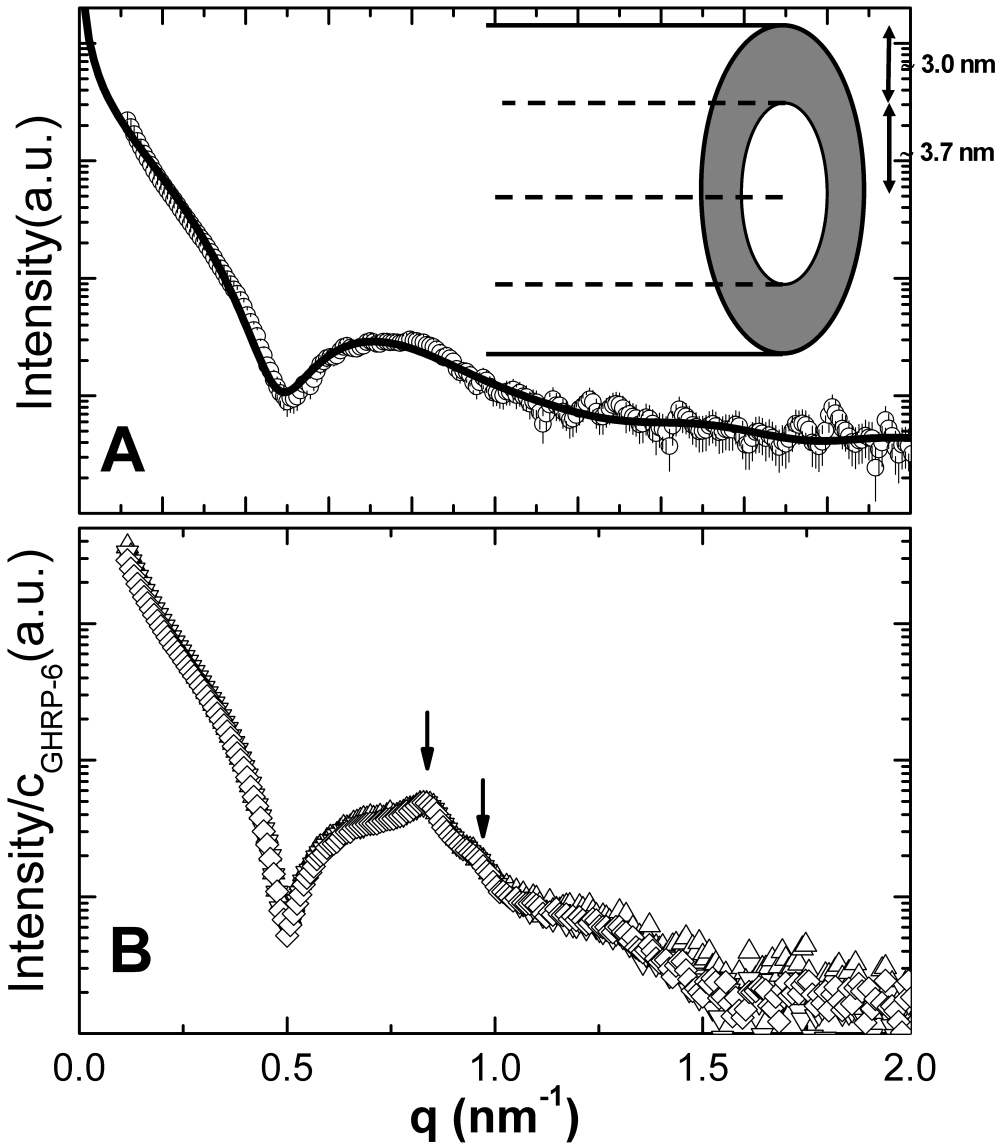

Fig. 3

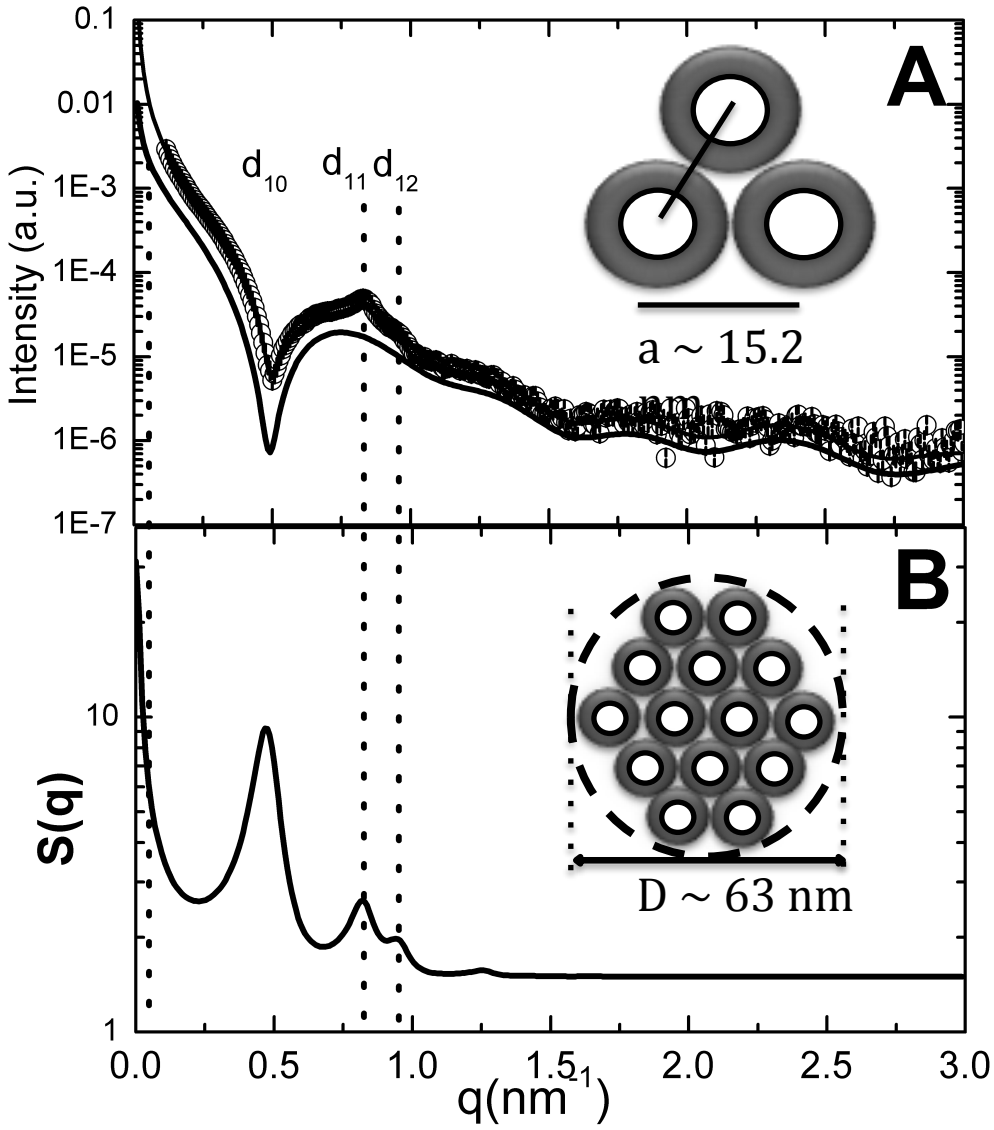

Fig. 4

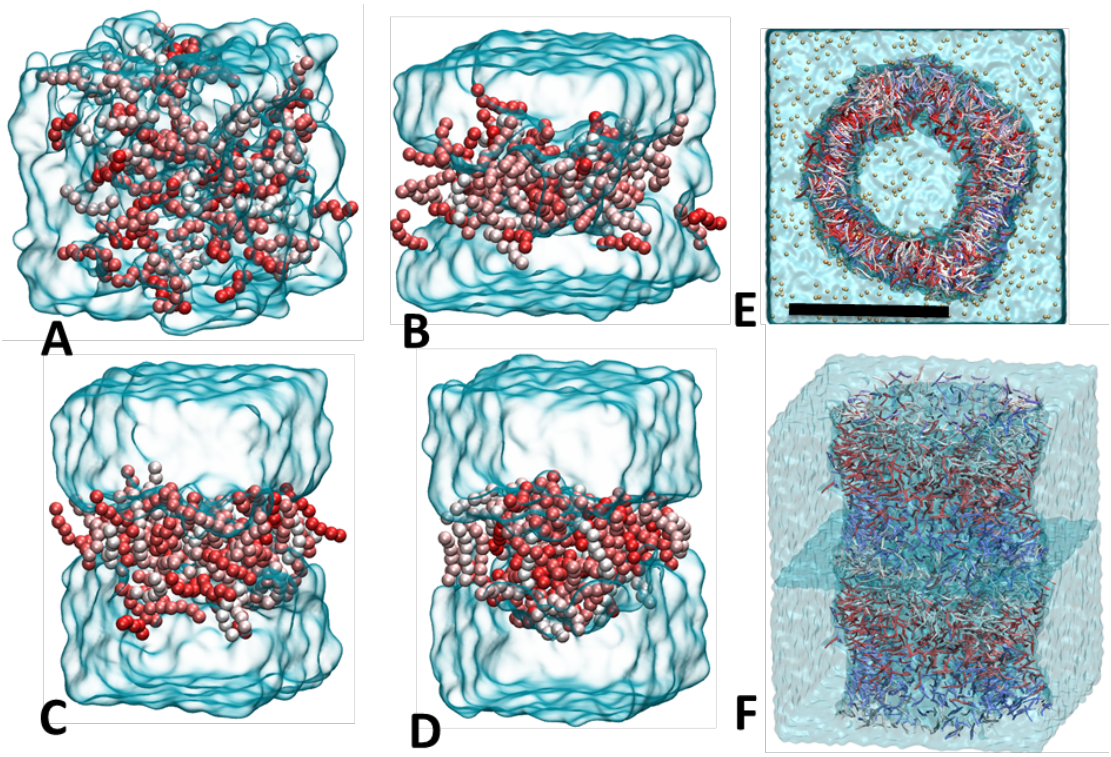

Figure 5

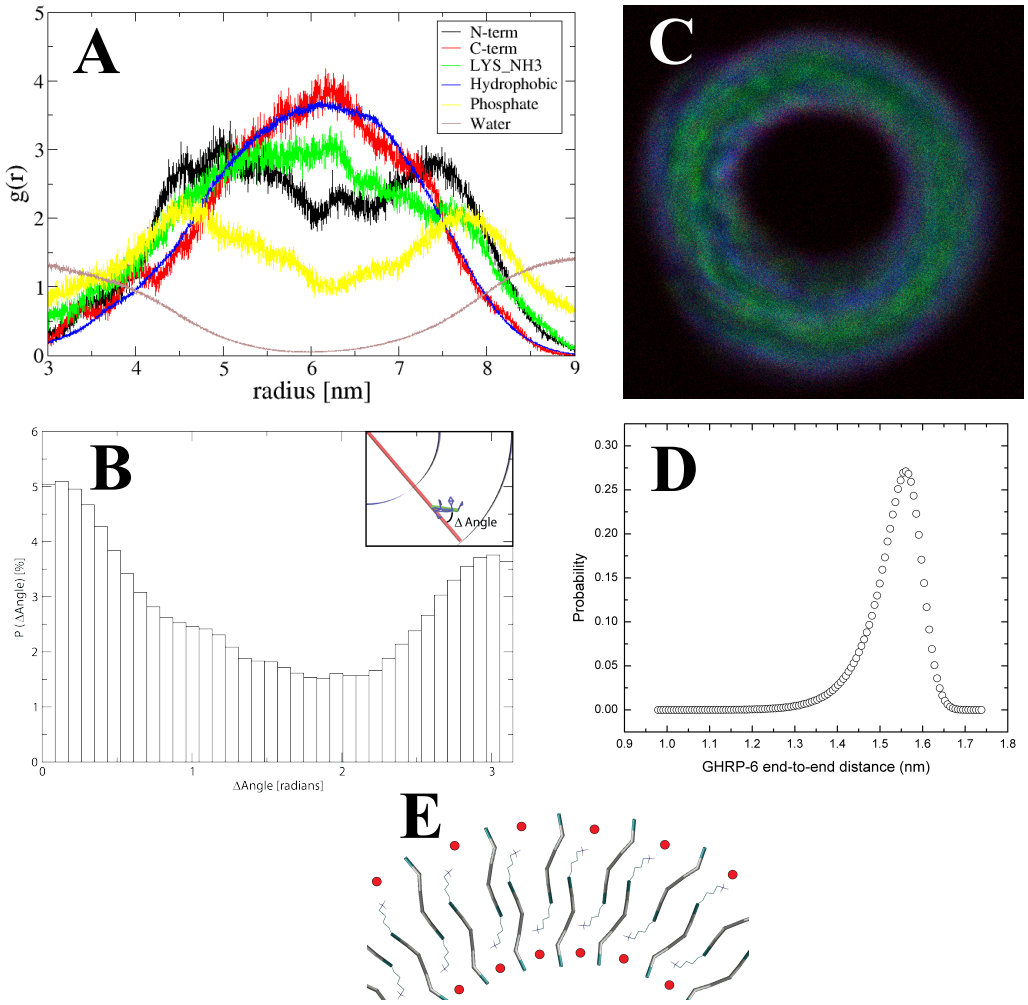

Figure 6